PAPER

High temperature structure evolution of SiBZrOC quinary polymer derived ceramics

Chen Liu, [ID] *[ab] Changqing Hong,[b] Xinwei Wang*[a] and Jiecai Han[b]

SiBZrOC quinary ceramics were obtained through the modification of a SiOC precursor with $B(OH)_3$ and $Zr(OnPr)_4$. The results showed that both B and Zr atoms were involved in the SiOC network through Si–O–B and Si–O–Zr bonds, respectively. The combined effects of B and Zr on the chemical structure and the thermal stability of the SiBZrOC system were investigated in detail. The sp^3–C/Si ratio of SiBZrOC ceramics was between the values for SiZrOC and SiBOC. The presence of B promotes the crystallization of t-ZrO_2, which precipitated at 1000 °C and transformed to m-ZrO_2 at 1400 °C. At 1600 °C, ZrO_2 reacted with the matrix and formed $ZrSiO_4$, which consumed SiO_2 and thus inhibited the carbothermal reaction. The very small $I(D)/I(G)$ ratio of 0.13 in the Raman spectra indicated the high graphitization of free carbon in SiBZrOC ceramics, which was observed by TEM with 10–20 graphene layers. The SiBZrOC ceramics showed excellent thermal stability in argon at 1600 °C for 5 h with a mass loss of 6%. Both the formation of $ZrSiO_4$ and the highly graphitized free carbon play important roles in inhibiting the carbothermal reaction and thus improving the thermal stability of SiBZrOC ceramics.

Introduction

Polymer-derived ceramics (PDCs) are attractive candidates for use under extreme conditions owing to their high strength, creep and thermal shock resistance, as well as stability in oxidative and corrosive environments. They are X-ray amorphous and comprised of nanodomains of different structures and compositions, obtained by the thermal decomposition of organic polymers. The most well-known classes of PDCs are the ternary systems SiCN and SiCO as well as the quaternary systems SiCNO, SiBCN, SiBCO, SiAlCN, and SiAlCO.[1–4] Usually, quaternary ceramics exhibit improved mechanical and thermal properties as compared to those of the ternary materials. Recent investigations have shown that the high temperature stability in terms of decomposition for the SiBCN ceramics can reach 2200 °C.[5]

The fabrication processes of these materials involve the preparation of precursors, pyrolysis and sintering. The modification of the precursor with B[6–8] and metallic elements such as Al,[9–11] Ti,[12,13] or Zr[14–16] Hf,[17–20] allows the design and controlled synthesis of multifunctional PDC materials with tailored properties. They are typically prepared by modifying precursors with metal alkoxides and subsequent ceramization, leading to SiOC/SiCN nanocomposites containing a finely dispersed metal oxide nanodomains. The nanodomains may significantly influence the microstructure and physical properties of these ceramics on a large scale, especially when the domains differ in their chemistry, electrical conductivity, and mechanical properties.[21–25]

Though early work already strongly suggested the nanoscale heterogeneity both in SiCO- and SiCN-based materials, the detailed chemical and structural nature of the quinary PDCs remained elusive. In previous work,[26,27] we prepared the B-modified and Zr-modified SiOC precursor through the chemical reactions of hybrid alkoxysilanes with boric acid and $Zr(OnPr)_4$, respectively. The results showed that the effects of B and Zr are contrary on some cases, such as the precipitation of SiC and the graphitization of free carbon. In this work, we synthesized a SiBZrOC quinary precursor by using the same raw materials and compared with previous work, to study the combined effects of B and Zr on the polymer-to-ceramic transformation processes and the microstructure evolution of SiBZrOC materials. Various characterization techniques such as NMR and Raman spectroscopy, X-ray diffraction, as well as TEM were used to study the structure of the metallo-organic precursor and the nanocomposites.[28–33]

Experimental

Methyltriethoxysilane (MTES), methyldiethoxysilane (MDES), boric acid ($B(OH)_3$) and $Zr(OnPr)_4$ (Alfa Aesar, 70 wt% in propanol) were used as the starting raw materials. MTES, MDES and $B(OH)_3$ was mixed with the molar ratio of MTES/MDES = 3 and B : Si = 0.4. The mixture was stirred until complete dissolution. The appropriate amount of $Zr(OnPr)_4$ was then added to the

[a]Laboratory for Space Environment and Physical Science, Harbin Institute of Technology, Harbin, 150001, PR China. E-mail: liuchen2016@hit.edu.cn; xinweiwang@hit.edu.cn

[b]National Key Laboratory of Science and Technology on Advanced Composites in Special Environments, Harbin Institute of Technology, Harbin 150001, PR China

Paper

prehydrolyzed solution under fast stirring with the molar ratio of Zr : Si = 0.2. The mixture was obtained and heated at 80 °C for 1 day for gelation. The SiBZrOC gel were dried at 80 °C for 2 days, grounded and finally sieved to <75 μm. The SiBZrOC precursor was finally obtained and pyrolyzed in a tube furnace with a heating rate of 5 °C min^{-1} in flowing argon gas, at 1000 °C, 1200 °C, 1400 °C, and 1600 °C for 1 h, followed by furnace cooling to ambient temperature.

TG were performed on the xerogels using a PerkinElmer differential scanning calorimeter from room temperature to 1400 °C at a heating rate of 10 °C min^{-1} under argon atmosphere. FTIR spectra of the precursor were recorded between 4000 and 400 cm^{-1} on a PerkinElmer Spectrum One FTIR spectrometer. NMR spectrum of precursor and ceramics was collected using a 4 mm Bruker CP MAS probe and a Bruker Ultrashield 300 MHz solid-state spectrometer. ^{29}Si CP MAS Powder samples were taken in ZrO_2 rotors and were spun at a rate of 5 kHz. The spectrum was collected using 30° pulses length of 4 μs and 2 s recycle delay. For each ^{29}Si NMR spectrum, 4000–90 000 transients were accumulated with a spectral width of 59 kHz. XRD patterns of ceramics were collected using a Philips X'Pert diffractometer with Cu Kα radiation. A 2θ range of 10–90° was scanned with a step size of 0.05°. Raman spectra were collected on a Raman Station (B&WTEK, BWS435-532SY) with a near infrared laser operating at 532 nm. The microstructure of the ceramics was observed using scanning electron microscopy (Helios Nanolab600i). A Philips-FEI Tecnai G2 F30 instrument was used to perform TEM investigations on the ceramic powders dispersed on copper grid.

Results and discussion

The TG/DTG curves of SiBZrOC precursor was shown in Fig. 1. The weight loss occurred mainly in three stages in the temperature intervals 50–200 °C, 200–500 °C, and 500–800 °C, respectively. The DTG curve shows an intense peak at 100 °C corresponding to a weight loss of 6 wt%, which is attributed to the loss of water and ethanol. The second weight loss of 7 wt% in the range of 200–500 °C, is probably related to the release of boric acid, H_2, and CH_4 as the predominant volatiles. In the third step, the weight loss of 4% is mainly due to the evolution of methane Si–CH$_3$. At above 800 °C, the weight remains unchanged and the ceramic yield was found to be 83%.

Fig. 2 shows the infrared spectra of SiBZrOC precursor and ceramics pyrolyzed at 1000 to 1600 °C. All the spectra show the characteristic peak of Si–O–Si bond between 1000 and 1130 cm^{-1}, which is split into two bands at 1035 and 1125 cm^{-1}, indicating the high degree of polymerization of the precursors. Si–O–Zr bond at 905 cm^{-1} was detected in the precursor formed through reactions (1) and (2), whilst disappeared in the ceramics owing to the redistribution reaction between Si–O and Zr–O bonds and thus formed Zr–O–Zr bonds. Si–O–B bond at 875 cm^{-1} was found in the ceramics, whilst absent in the precursor. This is probably because the Si–O–B bond has been formed through reaction (3) in the precursor, but covered up by the Si–O–Zr bond in the ceramics. The FTIR results confirmed
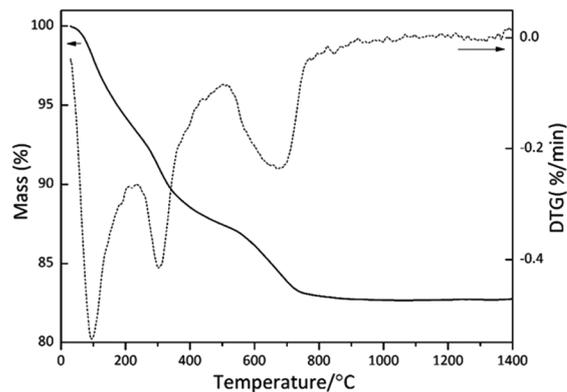

Fig. 1 TG curves of SiBZrOC precursor.

that both B and Zr were involved in the siloxane network in the SiOC network in the ceramics.

$$\equiv\!Si\!-\!OH + \equiv\!Zr\!-\!OPr \rightarrow \equiv\!Si\!-\!O\!-\!Zr\!\equiv + C_3H_7OH \quad (1)$$

$$\equiv\!Si\!-\!OH + \equiv\!Zr\!-\!OH \rightarrow \equiv\!Si\!-\!O\!-\!Zr\!\equiv + H_2O \quad (2)$$

$$Si\!-\!OH + B(OH)_3 \rightarrow Si\!-\!O\!-\!B + H_2O \quad (3)$$

Fig. 3 shows the ^{29}Si NMR spectra of SiOC, SiBOC, SiZrOC and SiBZrOC precursor. The spectra of SiOC and SiBOC precursor present a sharp signal at −69 ppm assigned to $SiCO_3$ units and another peak at −39 ppm due to $HSiCO_2$ units, whilst the latter was absent in SiZrOC and SiBZrOC precursor, revealing that the Si–H bonds has been transformed into Si–O bonds through reactions (4) and (5) in Zr-containing precursor.[26] Moreover, the $SiCO_3$ peaks in SiZrOC and SiBZrOC precursor were simulated with two Gaussian peaks at −62.7 and −69 ppm, which were assigned to the $SiCO_3$ units with and without Si–O–Zr bonds, respectively. The former unit accounts for 50% in SiBZrOC, which is obviously lower than the 74% in SiZrOC ceramics,[26] suggesting that the $SiCO_3$ units with Si–O–B bond in SiBZrOC accounts for 24% at most. The formation of
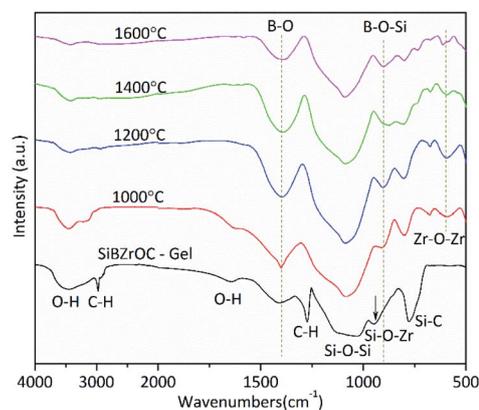

Fig. 2 Infrared spectra of SiBZrOC xerogel and ceramics pyrolyzed at various temperatures.
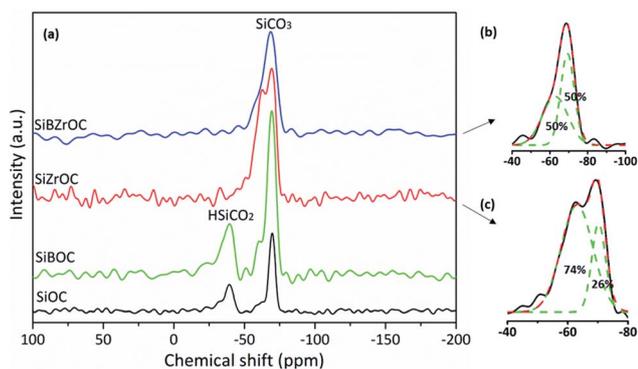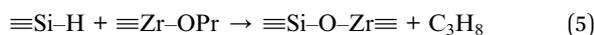
Fig. 3 ^{29}Si MAS NMR spectra of SiOC, SiBOC, SiZrOC and SiBZrOC precursor.[26,27]

Fig. 5 ^{29}Si MAS NMR spectra of SiOC, SiZrOC, SiBOC and SiBZrOC ceramics pyrolyzed at 1200 °C.[26,27]

Si–O–B bonds consumed a part of Si–O bonds and thus decreased the content of Si–O–Zr bonds. Combined with the FTIR results, it is confirmed that Zr and B was distributed uniformly in the SiOC network at atomic scale.

$$\equiv Si–OH + \equiv Zr–OH \rightarrow \equiv Si–O–Zr\equiv + H_2 \quad (4)$$

$$\equiv Si–H + \equiv Zr–OPr \rightarrow \equiv Si–O–Zr\equiv + C_3H_8 \quad (5)$$

As comparison, TG curves of SiOC, SiBOC and SiZrOC[26,27] precursor were shown in Fig. 4. The ceramic yield of SiBZrOC is 83%, much lower than the 93% of SiBOC, and slightly higher than the 81% of SiZrOC. This is probably because the formation of Si–O–B bond lead to a more interconnected gel network,[34] and thus higher ceramic yield in B-containing precursors. Compared with SiZrOC, the ceramic yield of SiBZrOC was slightly improved owing to the Si–O–B bonds formed through the 24% Si–O bonds.

The ^{29}Si MAS NMR spectra of SiBZrOC ceramics pyrolyzed at various temperature are presented in Fig. 5. All the spectra show the resonance peaks of SiO_4 ($\delta = -110$ ppm) and SiC_4 ($\delta = -15$ ppm) units, resulting from the redistribution reaction between
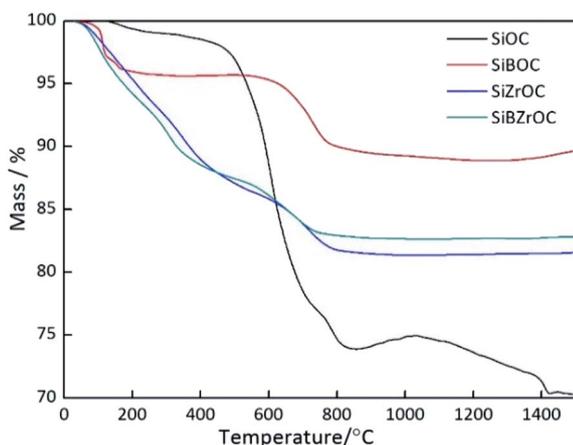
Si–O and Si–C bond. The sp[3]–C/Si ratio of the four ceramics were calculated according to the peak area of SiO_4 and SiC_4, listed in Table 1. It can be seen that the sp[3]–C/Si ratio of SiZrOC ceramics is 0.12, lower than the 0.16 of SiOC ceramics, which is attributed to the addition of Zr atom, leading to a decrease in the thermal stability of Si–C bond.[15] The SiBOC ceramics is 0.27, much higher than that of SiOC ceramics.[26] This is because the presence of Si–H groups in the precursor promotes the insertion of C into SiCO network[26] and the redistribution reaction between B–C and Si–O bond could also lead to the increase of sp[3]–C.[35] The sp[3]–C/Si ratio in SiBZrOC ceramics is 0.22, between the value of SiBOC and SiZrOC, resulting from the combined effects of B and Zr.

XRD patterns of SiBZrOC ceramics pyrolyzed at various temperatures are presented in Fig. 6. At 1000 and 1200 °C, t-ZrO_2 phase is found as the only crystalline phase in SiBZrOC ceramics. Small amounts of m-ZrO_2 were detected at 1400 °C, which was formed through the phase transformation from t-ZrO_2 during cooling down when the t-ZrO_2 grew up to the critical size.[26] It can be seen that the phase transformation temperature for SiBZrOC is 1400 °C, much lower than the 1600 °C for SiZrOC,[26] revealing the growth of t-ZrO_2 in SiBZrOC are faster than SiZrOC. Therefore, it can be concluded that the addition of B facilitates the growth of t-ZrO_2 crystallites. Moreover, ZrSiO_4 was found at 1600 °C, formed by the reaction of zirconia with amorphous silica in the matrix.

Fig. 7 shows the Raman spectra of SiBZrOC ceramics pyrolyzed at various temperatures. All the Raman spectra show two characteristic features of disordered graphitic forms of carbon: the D band at about 1350 cm^{−1} due to the defects and the G

Fig. 4 TG curves of SiOC, SiBOC, SiZrOC and SiBZrOC ceramics.[26,27]

Table 1 Calculated sp[3]/C ratio of SiOC SiZrOC[26] SiBOC and SiBZrOC ceramics pyrolyzed at 1200 °C

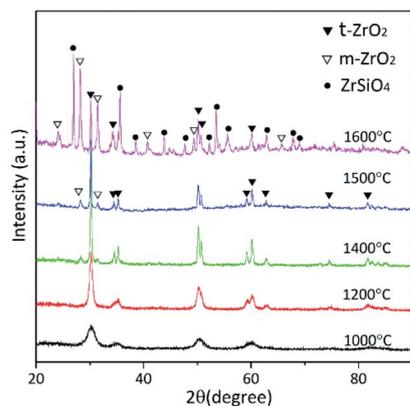| Ceramics	sp[3]–C/Si
SiOC	0.16
SiZrOC	0.12
SiBOC	0.27
SiBZrOC	0.22

Fig. 6 XRD patterns of SiBZrOC ceramics pyrolyzed at various temperatures.

band at 1590 cm^{-1} related to in-plane bond stretching of sp^2 carbon. The G band narrows from 47 cm^{-1} to 21 cm^{-1} and shifts to the lower frequencies, suggesting the increasing graphitization of free carbon with temperature.

The D band appears due to the A$_{1g}$ breathing mode and requires a defect for its activation. In our case, the D band is possibly related to carbon dangling bonds or sp^3 carbon atoms. The intensity ratio of D and G bands, $I(D)/I(G)$, reflects the graphitization of carbon materials, and it decreased with increasing graphitization. The diameter of free carbon cluster can be calculated using eqn (6),[36,37] shown in Table 2. The intensity of G band increases dramatically at above 1600 °C, and accordingly the $I(D)/I(G)$ rapidly decreases to 0.13 at 1600 °C, which leads to a large L_a of 38.1 nm.

$$\frac{I_D}{I_G} = \frac{C(\lambda)}{L_a} \tag{6}$$

Usually, the value of $I(D)/I(G)$ for SiBOC ceramics is more than 1 at below 1600 °C. In our case, the intensity of G band increases dramatically at above 1400 °C, and accordingly the
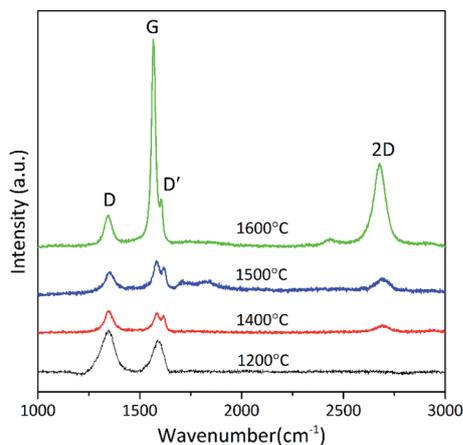
Table 2 Raman spectra parameters for SiBZrOC ceramics pyrolyzed at various temperatures

Temperature (°C)	$I(D)/I(G)$	ωG (cm^{-1})	FWHM (cm^{-1})	L_a (nm)
1200	1.3	1598	47	3.8
1400	1.2	1583	39	4.1
1500	0.69	1583	31	7.2
1600	0.13	1576	21	38.1

$I(D)/I(G)$ decreases to 0.13 at 1600 °C, which is far smaller than that in SiZrOC ceramics ($I(D)/I(G) = 1.4$). The results indicate that the addition of B significantly promotes the graphitization and the growth of free carbon cluster. This is probably owing to the partial substitution of C with B atoms, which could increase the crystallinity of carbon.[37,38] The D′ bands at 1608 cm^{-1} is considered to be the fingerprint of BC$_3$ site formed by the substitution of B for C atom.[9] This substitution of C by B atom introduces a local distortion within the graphite layer planes, and thus formed crystalline defects. The electron deficiency of boron with respect to carbon causes a decrease in the repulsive interaction between the π-electron clouds of adjacent graphene layers, allowing these layers to come closer together, and thus lead to the increased graphitization degree of free carbon.[37,38]

Backscattered electron images of the fracture of SiBZrOC ceramics pyrolyzed at 1000 °C, 1200 °C, 1400 °C and 1600 °C are shown in Fig. 8. Combined with XRD results, the white grains precipitated at 1200 °C with a size of 30–80 nm were t-ZrO$_2$. The spherical grains uniformly dispersed in the matrix and grew up to 200–350 nm at 1600 °C, which were supposed to be t-ZrO$_2$, m-ZrO$_2$ and ZrSiO$_4$ crystallites, according to XRD results.

Fig. 9 shows the TEM images and the corresponding diffraction patterns of SiBZrOC ceramics. The oval particle in the middle and the irregular particles in the upper are

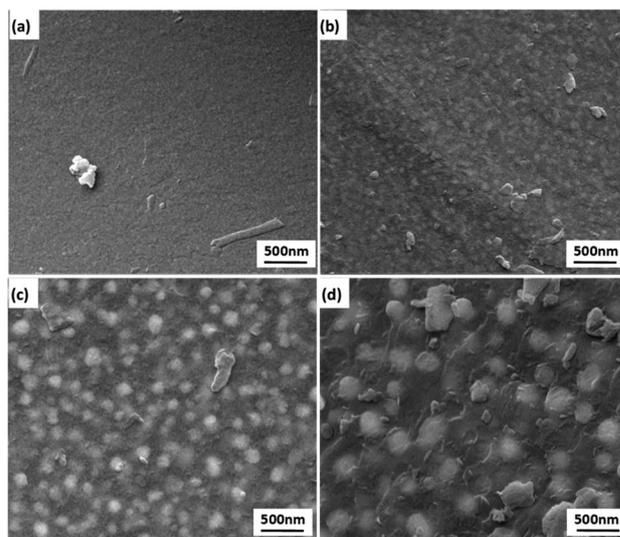**Fig. 7** Raman spectra of SiBZrOC ceramics pyrolyzed at various temperatures.

Fig. 8 SEM images of SiBZrOC ceramics pyrolyzed at (a) 1000 °C, (b) 1200 °C, (c) 1400 °C and (d) 1600 °C.
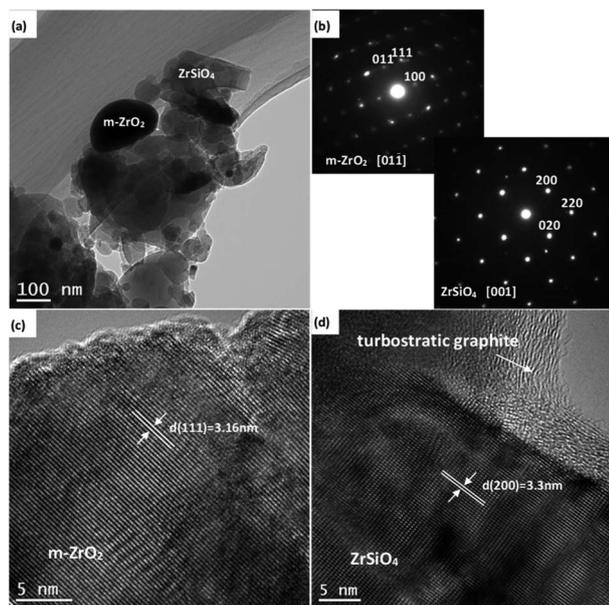
Fig. 9 TEM images of SiBZrOC ceramics pyrolyzed at 1600 °C. (a) Bright field image, (b) diffraction patterns, (c) and (d) high-resolution micrographs.

Table 3 Mass loss of SiZrOC and SiBZrOC ceramics pyrolyzed at 1200 °C after annealing in argon at 1400 °C, 1500 °C and 1600 °C for 5 h

Temperature (°C)	Mass loss	
	SiZrOC	SiBZrOC
1400	1%	1%
1500	4%	3%
1600	10%	6%

a high ceramic yield of 83% was achieved. The addition of B promoted the crystallization of ZrO_2 and the graphitization of free carbon, as well as increased the sp^3–C/Si ratio. t-ZrO_2 precipitated at 1200 °C with a size of 30–80 nm, reacted with the matrix and thus formed $ZrSiO_4$ at 1600 °C. Turbostratic graphite with 10–20 graphene layers was clearly observed in TEM. The SiBZrOC sample showed excellent thermal stability in argon at 1600 °C for 5 h with a mass loss of 6%. Both the formation of $ZrSiO_4$ and the highly graphitized free carbon inhibited the carbothermal reaction and thus improved the thermal stability of SiBZrOC ceramics.

Conflicts of interest

The authors confirm that the content of this article has no conflicts of interest.

Acknowledgements

Notes and references

1 S. Fu, M. Zhu and Y. Zhu, J. Adv. Ceram., 2019, 8, 457–478.
2 G. Mera, A. Navrotsky and S. Sen, J. Mater. Chem. A, 2013, 1, 3826–3836.
3 E. Erdem, V. Mass, A. Gembus, A. Schulz, V. Liebau-Kunzmann, C. Fasel, R. Riedelf and R. Eichel, Phys. Chem. Chem. Phys., 2009, 11, 5628–5633.
4 I. Menapace, G. Mera, R. Riedel, E. Erdem, R. Eichel, A. Pauletti and G. A. Appleby, J. Mater. Sci., 2008, 43, 5790–5796.
5 P. Zhang, D. Jia, Z. Yang, X. Duan and Y. Zhou, J. Adv. Ceram., 2012, 1, 157–178.
6 G. D. Soraru, N. Dallabona, C. Gervais and F. Babonneau, Chem. Mater., 1999, 11, 910–919.
7 R. Pena-Alonso, G. Mariotto, C. Gervais, F. Babonneau and G. D. Soraru, Chem. Mater., 2007, 19, 5694–5702.
8 A. Schiavon, C. Gervais, F. Babonneau and G. D. Soraru, J. Am. Ceram. Soc., 2004, 87, 203–208.
9 B. Julian, C. Gervais, E. Cordoncillo, P. Escribano, F. Babonneau and C. Sanchez, Chem. Mater., 2003, 15, 3026–3034.
10 X. Li and M. J. Edirisinghe, Chem. Mater., 2004, 16, 1111–1119.
11 T. Xu, Q. Ma and Z. Chen, Mater. Lett., 2012, 66, 364–366.
12 L. Crouzet, D. Leclercq, P. H. Mutin and A. Vioux, Chem. Mater., 2003, 15, 1530–1534.
13 S. Dire, R. Ceccato and F. Babonneau, J. Sol-Gel Sci. Technol., 2005, 34, 53–62.
14 E. Ionescu, C. Linck, C. Fasel, M. Müller, H. J. Kleebe and R. Riedel, J. Am. Ceram. Soc., 2010, 93, 241–250.

determined to be m-ZrO_2 and the $ZrSiO_4$, respectively, through the diffraction patterns in Fig. 9(b). They are well-crystallized as shown in the HRTEM images Fig. 8(c) and (d). Fig. 8(d) shows the typical turbostratic structure of free carbon with 10–20 graphene layers, which is rarely found in the SiZrOC ceramics.[26] It is confirmed that the addition of B significantly promotes the graphitization of free carbon.

Table 3 shows the mass loss of SiZrOC and SiBZrOC ceramics pyrolyzed at 1200 °C after annealing in argon at 1400 °C, 1500 °C and 1600 °C for 5 h. The SiBZrOC sample shows a mass loss of 6% compared with the SiZrOC sample of 10%, indicating the enhanced thermal stability in SiBZrOC. This can be attributed to the highly graphitized free carbon and the reaction of SiO_2 and ZrO_2, which both inhibit the carbothermal reaction between SiO_2 and free carbon.

Conclusions

SiBZrOC quinary ceramics was prepared through the chemical reactions of hybrid alkoxysilanes with boric acid and Zr(OnPr)$_4$. Si–O–Zr and Si–O–B bonds were formed in the precursor and

15 S. Dire, R. Campostrini and R. Ceccato, *Chem. Mater.*, 1998, **10**, 268–278.

16 S. Dire, R. Ceccato, S. Gialanella and F. Babonneau, *J. Eur. Ceram. Soc.*, 1999, **19**, 2849–2858.

17 E. Ionescu, B. Papendorf, H. Kleebe, F. Poli, K. Müller and R. Riedel, *J. Am. Ceram. Soc.*, 2010, **93**, 1774–1782.

18 E. Ionescu, B. Papendor, H. Kleebe, F. Poli, K. Müller and R. Riedel, *J. Am. Ceram. Soc.*, 2010, **9**, 1783–1789.

19 H. Kleebe, K. Nonnenmacher, E. Ionescu and R. Riedel, *J. Am. Ceram. Soc.*, 2012, **95**, 2290–2297.

20 K. Nonnenmacher, H. Kleebe, J. Rohrer, E. Ionescu and R. Riedel, *J. Am. Ceram. Soc.*, 2013, **96**, 2058–2060.

21 B. Papendorf, K. Nonnenmacher, E. Ionescu, H. Kleebe and R. Riedel, *Small*, 2011, **7**, 970–978.

22 E. Ionescu, H. Kleebe and R. Riedel, *Chem. Soc. Rev.*, 2012, **41**, 5032–5052.

23 F. Li, X. Huang, J. X. Liu and G. J. Zhang, *J. Adv. Ceram.*, 2020, **9**, 1–16.

24 P. Colombo, G. Mera, R. Riedel and G. D. Soraru, *J. Am. Ceram. Soc.*, 2010, **93**, 1805–1837.

25 N. Srinivasan, S. Ravindran and K. Ravi, *J. Am. Ceram. Soc.*, 2013, **2**, 318–324.

26 C. Liu, R. Pan, C. Hong, X. H. Zhang, W. Han, J. Han and S. Du, *J. Eur. Ceram. Soc.*, 2016, **36**, 395–402.

27 X. Zhang, C. Liu, C. Hong, J. Han, W. Han and S. Du, *Ceram. Int.*, 2015, **41**, 15292–15296.

28 S. J. Widgeon, S. Sen, G. Mera, E. Ionescu, R. Riedel and A. Navrotsky, *Chem. Mater.*, 2010, **22**, 6221–6228.

29 S. J. Widgeon, G. Mera, Y. Gao, E. Stoyanov, S. Sen, A. Navrotsky and R. Riedel, *Chem. Mater.*, 2012, **24**, 1181–1191.

30 G. Mera, A. Navrotsky, S. Sen, H. Kleebe and R. Riedel, *J. Mater. Chem. A*, 2013, **1**, 3826–3836.

31 G. Hasegawa, K. Kanamori, K. Nakanishi and T. Hanada, *J. Mater. Chem.*, 2009, **19**, 7716–7720.

32 G. Hasegawa, K. Kanamori, K. Nakanishi and T. Hanada, *Chem. Mater.*, 2010, **22**, 2541–2547.

33 Y. Shi, Y. Wan, Y. Zhai, R. Liu, Y. Meng, B. Tu and D. Zhao, *Chem. Mater.*, 2007, **19**, 1761–1771.

34 G. D. Soraru, R. Campostrini and S. Maurina, *J. Am. Ceram. Soc.*, 1997, **80**, 999–1004.

35 C. Gervais, F. Babonneau, N. Dallabonna and G. D. Sorarù, *J. Am. Ceram. Soc.*, 2001, **84**, 2160–2164.

36 T. Jiang, Y. Wang, Y. Wang and N. Orlovskaya, *J. Am. Ceram. Soc.*, 2009, **92**, 2455–2458.

37 M. Li, L. Cheng, F. Ye, C. Zhang and J. Zhou, *J. Adv. Ceram.*, 2021, **10**, 1256–1272.

38 Y. J. Lee, *J. Nucl. Mater.*, 2004, **325**, 174–179.